Scattering at magnetic and nonmagnetic impurities on surfaces with strong spin-orbit coupling

D. Lükermann,[1] S. Sologub,[2] H. Pfnür,[1] C. Klein,[3] M. Horn-von Hoegen,[3] and C. Tegenkamp[1,*]

[1]*Institut für Festkörperphysik, Leibniz Universität Hannover, Appelstraße 2, 30167 Hannover, Germany*

[2]*Institute of Physics, National Academy of Sciences of Ukraine, Nauky Avenue 46, 03028 Kyiv, Ukraine*

[3]*Department of Physics and Center for Nanointegration, Duisburg-Essen (CeNIDE), Universität Duisburg-Essen, Lotharstraße 1, 47057 Duisburg, Germany*

(Received 12 July 2012; published 28 November 2012)

Adsorption-induced reduction of surface-state conductivity in epitaxial Bi(111) films, a prototype system with large Rashba-induced surface-state splitting, by adsorbed atoms of Bi, Fe, and Co has been investigated by macroscopic surface magnetotransport measurements at a temperature of 10 K. A detailed analysis of magnetotransport, dc transport, and Hall data reveals that the scattering efficiencies for Co and Fe are larger by a factor of 2 than that for Bi. While for the latter charge transfer and change of band filling near the Fermi level are negligible, we find an increase of hole concentration upon Co and Fe adsorption. These atoms act as acceptors and immobilize on average about 0.5 electrons per adsorbed atom. Besides the dominant classical magnetoconductance signal the films show signatures of weak antilocalization, reflecting the strong spin-orbit coupling in Bi(111) surface states. This behavior can be changed to weak localization by the adsorption of high concentrations (0.1 monolayers) of magnetic impurities (Fe,Co), similarly to results found on the topological insulator Bi_2Se_3. Our results demonstrate that details of chemical bond formation for impurities are crucial for local spin moments and electronic scattering properties.

DOI: 10.1103/PhysRevB.86.195432 PACS number(s): 73.50.Jt, 68.43.−h, 75.30.Hx, 73.50.−h

I. INTRODUCTION

Magnetoelectrical effects like the giant magnetoresistance,[1] the spin Hall effect,[2] or the Datta-Das transistor[3] rely on the control and manipulation of spin-polarized currents. In order to study fundamental aspects in the field of spintronics, surfaces with strong spin-orbit coupling (SOC) came lately into the focus of research, since the loss of space-inversion symmetry at surfaces favors formation of spin-polarized surface band structures.[4–6] Recently, this material class has been expanded to metal/semiconductor systems with giant Rashba effects [e.g., Pb/Ge(111)].[7] Topological insulators,[8,9] on the other hand, reveal nontrivial, robust, and linearly dispersing surface states [e.g., Bi_2Se_3,Bi_2Te_3 (Refs. 9 and 10)]. All these systems have in common that elastic and spin-conserving backscattering from $+k$ to $-k$ states of propagating electrons near the Fermi level E_F is strongly suppressed and in the case of topological insulators even forbidden, as a consequence of the chirality of the spin states and time-reversal (TR) symmetry.[11]

Many of these aspects can be studied using clean Bi surfaces[5,12,13] and, in particular, epitaxially grown Bi films on Si substrates.[14–19] Not only are the latter interesting because of the fabrication of high-quality films, but there are also indications that ultrathin Bi films (1–4 bilayers) reveal a nontrivial Z_2 topology.[20] The comparatively high Rashba parameter found[21] for Bi(111) ($\alpha = 0.55$) results in the formation of an anisotropic Fermi surface with electron pockets around the $\overline{\Gamma}$ point and of elongated hole lobes along the $\overline{\Gamma M}$ directions.[19] While most of the work has been done using spin- and angle-resolved photoemission spectroscopy, only little is known about the interplay between spin-orbit coupling and transport. Fortunately, the bands of inner layers in epitaxially grown ultrathin Bi(111) films contribute very little to electronic transport.[22] Therefore, mainly the surface states are responsible for the total conductance, at least for a film thickness of several nanometers, as deduced from the first surface-sensitive transport measurements using epitaxial Bi(111) films.[15–18,23] Indeed, as expected for the given spin texture of the surface band structure, the analysis of charge-density interference patterns by scanning tunneling microscopy (STM) and scanning tunneling spectroscopy (STS) (Ref. 14) has confirmed that backscattering, as defined above, is strongly suppressed in Bi systems, i.e., only spin-conserving scattering processes with asymmetric momentum transfer are visible. This is a result of the anisotropic Fermi surface of the Bi(111) system in conjunction with the spin-polarized surface bands. Because of this anisotropy, also the weak antilocalization (WAL) signal, expected for systems with strong spin-orbit coupling[24,25] and found for monolayer structures of Ag and Pb on Si substrates,[26,27] is small, as we will show below.

The basic idea of adsorption of atoms with magnetic moments is that locally the time-reversal symmetry is broken; hence the direct (spin-conserving) backscattering channel for electrons and holes is activated. Magnetotransport measurements on the topological insulator Bi_2Se_3 have shown that the incorporation of magnetic impurities can change the behavior of a system with strong spin-orbit coupling and suppressed backscattering from WAL to weak localization (WL) for quite large amounts of impurity atoms.[28] Furthermore, by adsorption of magnetic Fe impurities on Bi_2Se_3, a remarkable insensitivity for backscattering of the topological state is reported in the low-impurity-concentration regime.[29] Additional scattering channels are opened for magnetically doped topological insulators [$(Bi_{1-x}Fe_x)_2Te_3$, $x \approx 0.0025$].[30] All these studies show that incorporation of magnetic impurities is an important issue in this context. The concentration needed in order to see such effects is comparatively high: The bulk Fe concentration reported in Ref. 30 would correspond to a coverage of approximately 0.02 monolayers (ML) in two dimensions. However, the idea of breaking locally the TR symmetry contrasts with recent STM experiments. The analysis of STS maps of interference patterns around single manganese

phthalocyanine (MnPc) molecules with a large magnetic moment, physisorbed on a Bi(110) single-crystal surface, revealed only spin-conserving scattering events.[13]

In this study we report on changes of the effective carrier concentrations and of the corresponding mobilities for electrons and holes as well as of weak localization on the Bi(111) surface, induced by adsorption of magnetic and nonmagnetic impurities at low temperatures. Recently, we have shown that the study of magnetotransport allows a quantitative determination of all parameters relevant for transport of both electrons and holes in surface states.[15] The magnetoconductance (MC) curves are dominated by the classical magneto effect, i.e., by *incoherent* scattering, whereas coherent scattering is reflected in the small contribution by weak antilocalization. The classical MC behavior is still dominant after adsorption of either Fe, Co, or Bi atoms. While for Bi adatoms the concentrations of holes and electrons remain almost constant, the hole concentration is increased in case of Fe and Co adsorption, pointing towards strong hybridization with the substrate. Additionally the WAL behavior, found after subtraction of the classical curve for clean films, changes towards WL for large amounts of magnetic impurity Fe, whereas it stays unaltered in the case of Bi adsorption on the Bi film.

II. EXPERIMENTAL SETUP

For the conductivity measurements, low-doped Si(111) samples ($\rho > 1000\ \Omega\,\mathrm{cm}$) have been used as substrates for film growth. Details about the fabrication of contacts as well as the *in situ* cleaning procedures are described elsewhere.[15,31] Bi was evaporated using a ceramic crucible, while Fe and Co were evaporated by electron beam bombardment out of a tantalum crucible. The amounts were controlled by quartz microbalances. Bi films as templates for further adsorption experiments were grown at 200 K followed by annealing to 450 K for several minutes. The morphologies of the Si substrate and the Bi(111) films have been checked by low-energy electron diffraction (LEED) (the rhombohedral notation was used for indexing the Bi planes,[32] i.e., the surface normal coincides with the ⟨111⟩ direction). The layer thickness of the Bi films is given in bilayers ($\mathrm{BL} = 1.14 \times 10^{15}\ \mathrm{atoms/cm^2}$). The Bi coverage has been calibrated with the help of the $\sqrt{3} \times \sqrt{3}\ \beta$ (1/3 ML) and α phases (1 ML) on Si(111),[33] and by recording bilayer oscillations in conductance during evaporation of Bi at 10 K on annealed Bi films. Please note that the Bi excess coverage is assumed to adsorb as monomers and is given in monolayers ($1\ \mathrm{ML} = 5.57 \times 10^{14}\ \frac{\mathrm{atoms}}{\mathrm{cm^2}}$). In the cases of Co and Fe, the conductance curves reveal a minimum after 0.5 ML (again based on the Bi ML density) has been deposited at 10 K. This minimum is used as calibration for the deposited amount. For magnetotransport measurements the prepared Bi films are transferred *in situ* into the magnetic field (±4 T). The adsorption experiments as well as the magnetoconductance measurements were performed at 10 K, i.e., contributions from phonon scattering are not crucial.

III. RESULTS AND DISCUSSION

A representative LEED pattern obtained after preparation of a 20-BL-thick Bi film is shown in Fig. 1(a). The diffuse

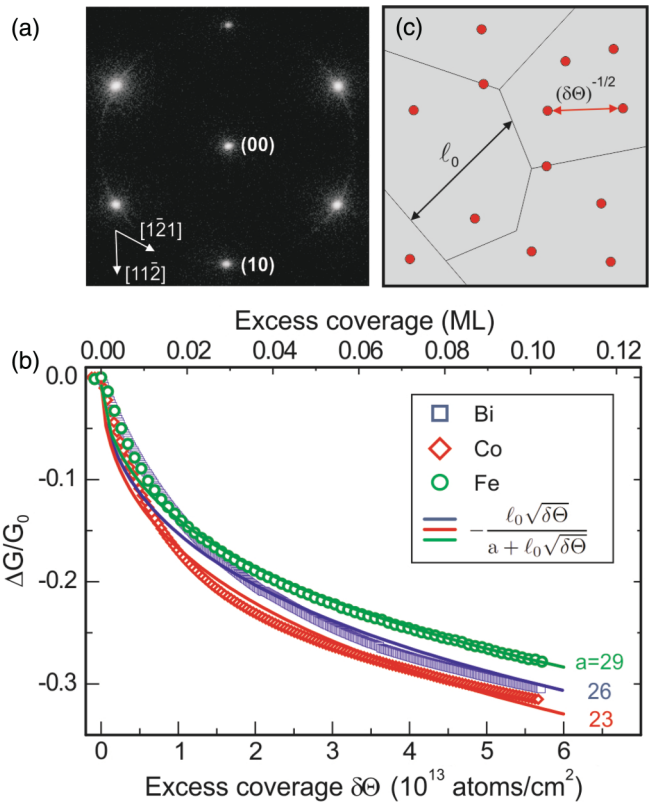

FIG. 1. (Color online) (a) LEED pattern of a 20 BL Bi(111) film grown on Si(111), which is the template for further adsorption studies. The electron energy of 96 eV is close to an out-of-phase scattering (step height 3.9 Å). (b) Change of conductance upon adsorption of various metals at 10 K on these films. The conductance of the clean surface G_0 was around 2 mS. The black solid lines are fits to the experimental data using Eq. (1). $\ell_0 = 15$ nm for all fits, corresponding to the mean grain size of the Bi films, deduced from a LEED investigation of the (00) spot. (c) Schematic drawing of the Bi(111) domain structure with some adsorbate atoms (circles) in order to illustrate the two characteristic length scales for the mean free path, ℓ_0 and $\ell \propto 1/\sqrt{\delta\Theta}$, respectively. For details see the text.

circular diffraction intensity around the first-order diffraction spots is due to the presence of rotationally disordered Bi domains. Further details are described elsewhere.[15,32,34] The conductance of these films is typically 2.0 ± 0.3 mS. However, the absolute values depend on domain sizes on the surface, which vary to some extent from sample to sample. As judged from the analysis of the full width at half maximum of the (00) diffraction spot, measured at different electron energies [so-called $H(S)$ analysis], the average domain size of the films studied here is typically around 15 nm. Thus, already for an excess coverage of $\delta\Theta \geqslant 0.001$ ML the mean free path is strongly influenced by scattering at the adatoms if one assumes randomly distributed monomers after adsorption at 10 K, separated by a mean adsorbate distance $1/\sqrt{\delta\Theta}$.

A. Adsorbate-induced changes in dc conductance

The relative change in conductance $\Delta G/G_0 = G(\delta\Theta)/G_0 - 1$ upon adsorption of different adsorbates in the coverage regime up to 0.1 ML is shown in Fig. 1(b). G_0 denotes the

conductance of the clean Bi(111) film. As clearly visible, the conductance decreases significantly when adatoms are adsorbed onto the freshly prepared Bi(111) surfaces. This supports the recent finding that indeed the surface states contribute to a large extent to the total conductance of the Bi(111) films.[15] Moreover, the scattering cross section depends on the deposited material. For instance, at 0.1 ML the relative change in conductance is as large as 32% for Co, while it is lower for Bi (30%) and Fe (27%). A minimum in conductance appears near a coverage of additional atoms of 0.5 ML, as expected for random two-dimensional (2D) growth.

The change in conductance can be accurately modeled by assuming elastic scattering processes of the surface carriers, and taking into account two characteristic length scales to be identified with the average domain size ℓ_0 and the average adatom separation $1/\sqrt{\delta\Theta}$ [in Fig. 1(c)]. The domain boundaries of the pristine Bi films determine a scattering time $\tau_0 = \ell_0/v_F$, where v_F is the (average) Fermi velocity, which results in the conductance G_0 of the clean film. After deposition of adatoms the scattering rate $1/\tau'$ increases to $1/\tau' = 1/\tau_0 + 1/\tau$. The scattering time $\tau = \ell/v_F$ is defined by the mean free path due to adsorbates, $\ell = a/\sqrt{\delta\theta}$. Thereby, the parameter a is given by the scattering probability at an impurity, $P = 1/a$.

The relative change of the conductance then reads

$$\Delta G/G_0 = -\frac{\ell_0\sqrt{\delta\Theta}}{a + \ell_0\sqrt{\delta\Theta}} \tag{1}$$

[compare with the thin solid lines in Fig. 1(b)]. The experimental data can be fitted well with this simple model in the low-coverage regime up to 0.1 ML. A more detailed description considering effects of nucleation can be found in Refs. 16 and 17, where the adsorption of Bi adatoms at 80 K on Bi(111) films has been studied. Assuming the mean free path ℓ_0 to be the same for all three deposition runs, we find the values for the probability of charge carriers to be scattered at an impurity atom to vary little ($P_{\mathrm{Fe}} = 1/29$, $P_{\mathrm{Bi}} = 1/26$, and $P_{\mathrm{Co}} = 1/23$).

However, the estimate of P_{Co} and P_{Fe} solely from the $G(\Theta)$ curves shown in Fig. 1(c) is misleading, because charge transfer plays a major role. As a result we will show that the scattering probability for Fe and Co is twice as large as for Bi ($P_{\mathrm{Co}} \approx P_{\mathrm{Fe}} \approx 2P_{\mathrm{Bi}}$). In order to shine light on these parameters and take into account the Rashba-split surface band structure, giving rise to electron and hole carriers, magnetotransport and Hall measurements will be presented in the following.

B. Adsorbate-induced changes in the classical magnetoconductance and Hall resistivity

As we will see in the following, the dominant contribution to magnetoconductance is given by incoherently scattered electrons, giving rise to the classical magneto effect. In addition, a small fraction of coherently backscattered electrons, giving rise to weak (anti)localization, is present, and will be in discussed separately in Sec. III C.

Common to all films investigated so far is the observation that the magnitude of the WAL contribution anticorrelates strongly with the quality of the films. The higher the (surface) mobility of the charge carriers, the smaller the signal of WAL. Particularly for epitaxially grown Bi(111) films, residual imperfections at the surface and in deeper layers are strongly interrelated and determine the quality of the film. Taking into account the large Fermi wavelengths involved here and the fact that quantum size effects turn deeper layers into insulators,[35] scattering of conduction electrons in surface states can happen both at surface defects and at defects in deeper layers. In this sense, there are "bulk"[36,37] and surface contributions to the resistivity. As a consequence, the bulk contribution to WAL does not depend on surface modifications, as recently shown by us.[15]

1. *Bi adsorption*

In this section, we concentrate on the classical magnetoresistance effect, which simply reflects the decrease of conductance due to the increase of the electron path at the surface in presence of a magnetic field applied perpendicular to the surface. Due to better film quality than in Ref. 15 the classical contribution dominates the B-field dependence of conductance even more strongly [for the separation of WAL, see the inset of Fig. 2(a)]. Measurements of magnetoconductance and Hall resistivities allow the separation of mobilities and charge carrier concentrations and their adsorption-induced changes, which is not possible from dc conductance alone. For the adsorption of Bi adatoms on Bi(111) films, charge transfer processes are expected to be small, and reduced carrier mobilities should be mainly responsible for the decrease in conductance discussed above. Figure 2(a) shows the change of the magnetoconductance $G(B) - G_0$ measured for different Bi adatom densities up to 0.12 ML. As the excess coverage increases the curvature of the magnetoconductance curves is gradually reduced. As shown recently, the curvature of the MC data is determined by the mobilities and carrier concentrations for electrons and holes in surface states, respectively.[15,23]

Qualitatively, the decrease of the curvatures just indicates a reduced mobility, in accordance with our expectations. The magnetoconductance curves can be accurately modeled using the two-carrier model for the surface-state-related transport.[38] For given electron and hole mobilities (μ_n and μ_p) and the ratio $c = p/n$, where p and n denote the hole and electron concentrations, respectively, the surface magnetoconductance $G(B)$ can be expressed by

$$G(B) = G_0 \frac{1 + (1-c)^2 \frac{\mu_n^2\mu_p^2}{(\mu_n + c\mu_p)^2} B^2}{1 + \mu_n\mu_p \frac{\mu_p + c\mu_n}{\mu_n + c\mu_p} B^2}. \tag{2}$$

Furthermore, the corresponding Hall resistivities $\rho_H = \frac{\pi}{\ln(2)} \frac{U_H}{I}$ (with the Hall voltage U_H and measurement current I) as a function of the magnetic field B for different Bi adatom densities are plotted in Fig. 2(b). Upon adsorption the slopes of the Hall resistivity reverse their sign. For a semimetallic system, where both electrons and holes contribute to the conductance, the Hall resistivity is given by

$$\rho_H(B) = -\frac{B}{|e|} \frac{n\mu_n^2 - p\mu_p^2 + (n-p)\mu_n^2\mu_p^2 B^2}{(n\mu_n + p\mu_p)^2 + (n-p)^2\mu_n^2\mu_p^2 B^2}, \tag{3}$$

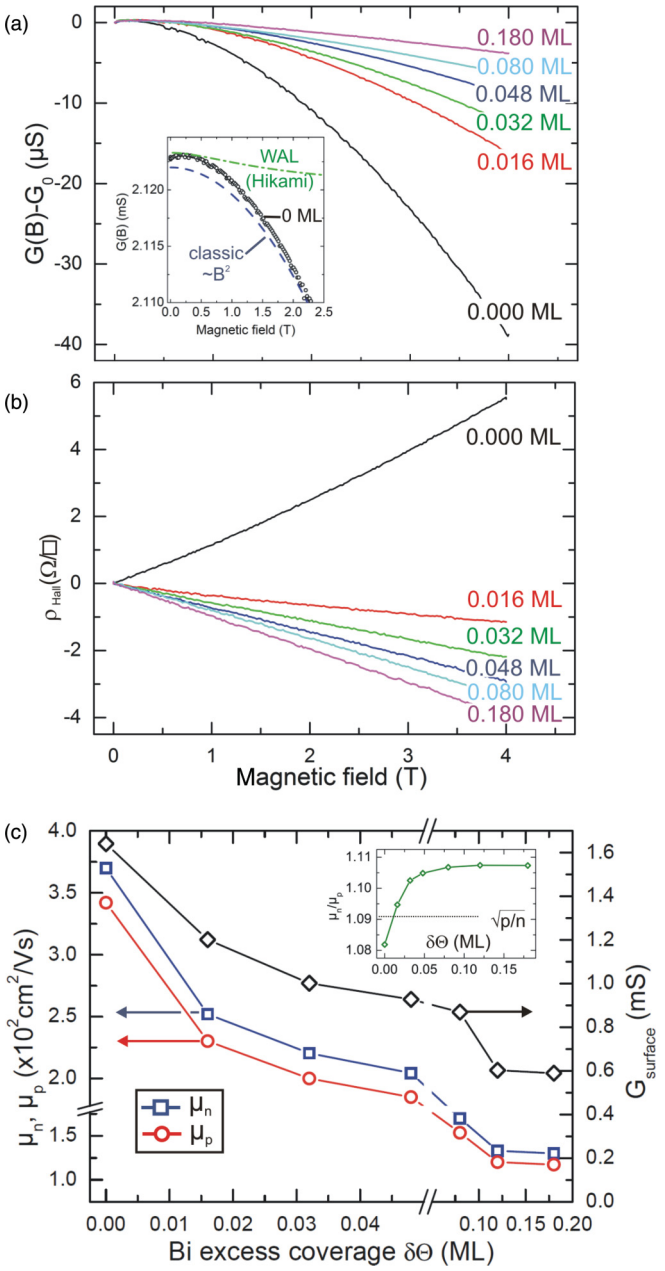

FIG. 2. (Color online) (a) Magnetoconductance (MC) curves for Bi on Bi(111) films for various concentrations of excess Bi adatoms. Inset: Magnified section at small B fields and zero excess coverage, demonstrating the contribution of WAL to the total magnetoconductance curves. (b) Corresponding Hall resistivity measurements. (c) Mobilities for electrons (μ_n, □) and holes (μ_p, ○) (left scale) and the calculated surface conductance $G = \sigma\pi/\ln 2$ (right scale, ◇) obtained from the simultaneous fit of the MC and Hall data. The inset shows the μ_n/μ_p ratio in order to illustrate the origin of the different slopes of ρ_H. For details see the text.

i.e., not only the type of carrier concentration (n, p) but also their mobilities (μ_n, μ_p) need to be considered in order to describe the slopes correctly.

In order to derive reasonable values for the carrier mobilities and concentrations the MC and Hall data have been fitted simultaneously, taking the effective masses from photoemission data.[18] Indeed, the carrier concentrations can be kept constant in the fit for all excess coverages at the values $n = 3 \times 10^{12}$ cm^{-2} and $p = 4 \times 10^{12}$ cm^{-2} for electrons and holes, respectively. These are the same as those found previously by us.[15] The mobilities obtained from the best fits for both carrier types are shown in Fig. 2(c). As expected, the mobilities of both charge carriers decrease with increasing density of the adatoms, but for holes more quickly than for electrons. The sign of the Hall resistivity depends crucially on the ratio of the mobilities. From Eq. (3) it is evident that for small magnetic fields the Hall resistivity depends linearly on the magnetic field; however, the slope of ρ_H is positive (negative) if $\mu_n/\mu_p < (>)\sqrt{p/n} = 1.09$. From the ratio of the mobilities plotted in the inset of Fig. 2(c) it is obvious why the Hall resistivity changes its sign upon adsorption although the carrier densities stay unaltered.

The surface-state conductance can now easily be calculated via $G(\theta) = \frac{\pi}{\ln 2} e[n\mu_n(\theta) + p\mu_p(\theta)]$ and is plotted in Fig. 2(c) as well. The qualitative agreement between the calculated [Fig. 2(c), $\Delta G/G_0|_{0.04\ \mathrm{ML}} = 0.37$] and measured [Fig. 1(b), $\Delta G/G_0|_{0.04\ \mathrm{ML}} = 0.22$] values supports the previous finding that the electron transport in thin Bi(111) films is carried to a large extent by the surface states whereas the bulk does not contribute. It should be noted that the conductance shown in Fig. 2(c) has been calculated from MC data, which are defined in the high-magnetic-field regime solely by surface-state properties, thus neglecting any bulk contributions. Besides bulk imperfections (see below), small charge transfer upon adsorption, which has been completely neglected in the analysis, might be responsible for the small discrepancy between measured and calculated values.

2. *Fe and Co adsorption*

In the context of Fig. 1 we have seen that the conductance of the Bi(111) surface state decreases as the monomer density of Bi, Fe, and Co increases. While the changes for Co were found in the dc transport measurements to be slightly larger than those for Bi, the change is marginally less in the case of Fe adsorption. However, the MC data shown for Fe and Co in Fig. 3 reveal a different picture. Concerning the magnetoconductance curves the changes after Fe and Co adsorption are even larger than those found for Bi adatoms. All curves are again dominated by classical magnetoconductance behavior. The classical behavior is exemplarily shown by dashed lines in Figs. 3(a) (0.028 ML Fe) and 3(c) (0 and 0.025 ML Co). The deviation of the data from these lines is again caused by WAL effects. WAL, and in particular its adsorbate-induced modification, will be discussed in the next section in more detail.

Regarding the Hall resistivity, we have seen in the case of Bi that the smallest amounts of excess coverage already lead to a change of slope, which is the result of an increased scattering probability for holes. According to the band structure, the Fermi wavelength for holes is shorter than for electrons. Therefore, holes scatter more efficiently at a given density of scatterers. Qualitatively, this phenomenon is reflected by the increase of the ratio between the two carrier mobilities as a function of excess coverage [cf. the inset of Fig. 2(c)]. The ρ_H behavior found in the cases of Fe and Co adsorption is different from that in Bi adsorption. Up to 0.025 ML and

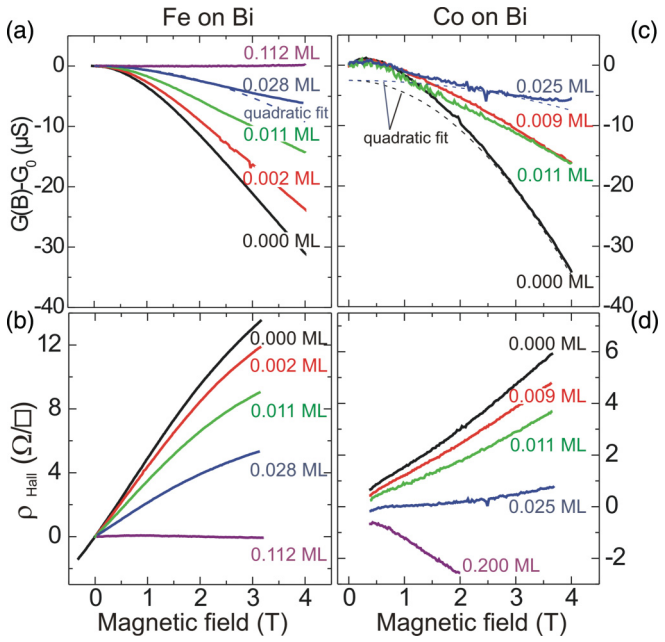

FIG. 3. (Color online) Magnetoconductance and Hall resistivity curves obtained after adsorption of Fe (a), (b) and Co (c), (d) on a 20-BL-thick Bi(111) film at 10 K. The best fits to the classical quadratic behavior of $G(B)$ are exemplarily shown by dashed lines in (a) and (c). The inset in (a) is an enlarged representation for $\delta\Theta = 0.112$ ML Fe, which shows drastic deviation from the classical trend, in qualitative agreement with the weak-localization theory of Hikami (dashed green). In (d), $\delta\Theta = 0.2$ ML, the data have been measured only up to 2 T. The corresponding $G(B)$ data are not shown in (c).

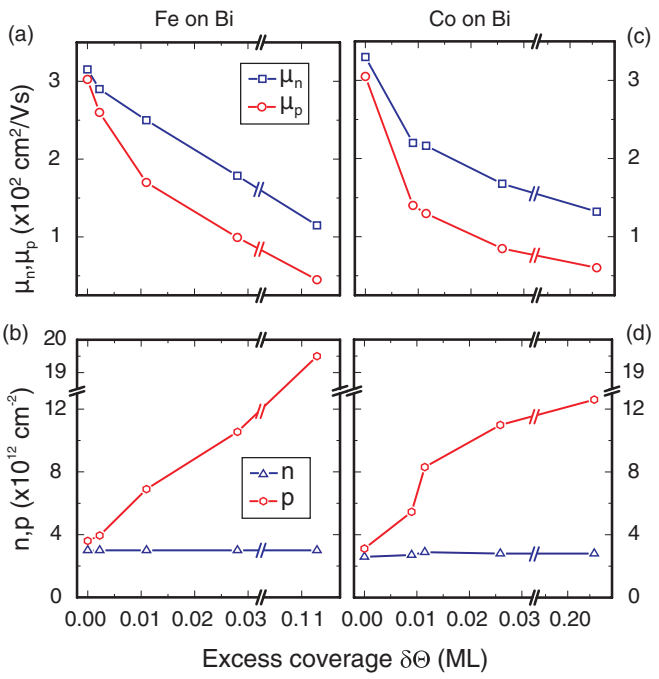

FIG. 4. (Color online) Electron (μ_n, □) and hole (μ_p, ○) mobilities for Bi(111) films with Fe (a) and Co (c) adatoms and their corresponding carrier concentrations (n, △) and (p, ⬡) (b), (d) deduced from the Hall and MC data shown in Fig. 3.

0.028 ML, respectively, the Hall resistivity is positive for all magnetic fields above 0.5 T. Only for high excess coverages (>0.1 ML) does the slope of the Hall resistivity as a function of the magnetic field change sign (in the case of Co) or become almost 0 (in the case of Fe). Taking into account the finding for Bi/Bi(111), discussed above in the context of Fig. 2(c), the behavior found for Fe/Bi(111) and Co/Bi(111) can be explained only if the hole concentration is changed drastically. This is indeed the result of the detailed analysis of the MC and Hall data, which will be presented in the following.

The MC data and the Hall measurements shown in Fig. 3 have been evaluated in a similar manner as the Bi data presented in the previous section. The mobilities for electrons and holes as well as the carrier concentrations deduced from the analysis are shown in Fig. 4 for both adsorbates. As expected, the mobilities decrease with increasing coverage. Again, the electron mobility μ_n is larger than the hole mobility μ_p. However, the reduction of mobilities induced by Fe and Co is nearly twice as large as for Bi [cf. Fig. 2(c)] after adsorption of 0.01 ML, although the initial reduction of conductance in the $G(\theta)$ measurements is almost identical [cf. Fig. 1(b)]. As we will show in the following, this effect is compensated by a modified carrier concentration upon adsorption.

While upon Bi adsorption the carrier concentrations within the Bi film remain constant over the entire adsorption range, this is different for Fe and Co adsorption as shown in Figs. 4(b) and 4(d). Again the p/n ratio for the clean surface is close to that found in the former case. However, the carrier concentrations change dramatically upon adsorption of Fe or Co. While the electron concentration is slightly reduced, the hole carrier density increases by a factor of 3–4 for both metals at a coverage of only 3% of a monolayer. ParticularlyIn particular, the strong increase seen in the low-coverage regime leads to the compensation of the strong decrease of the mobilities mentioned above. For the low-coverage regime (up to 0.03 ML) we conclude that each Fe atom localizes 0.5 ± 0.1 and every Co atom 0.6 ± 0.1 electrons from the bismuth surface states. Although photoemission data are missing for these adsorbates on Bi films so far, the observed behavior of carrier concentrations can be explained qualitatively only by adsorbate-induced modifications of the electronic band structure of the Bi surface states, as also found for topological insulators in the presence of magnetic impurities.[28] Furthermore, the fact that the curvature of the MC data changes dramatically compared to that for Bi and deviates from the classical shape for large Co and Fe concentration supports the model that for a critical Fe or Co coverage the spin-orbit coupling of the carriers in the surface states is modified more strongly than for Bi and TR symmetry is broken. The effects of weak localization and spin-orbit scattering are discussed in the following.

C. Weak localization and influence of magnetic atoms

As already shown above, the contributions of weak localization to magnetoconductance become visible only after subtraction of the classical contribution. The results are shown exemplarily for Fe and Bi adatoms in Figs. 5(a) and 5(c), respectively. For all measurements the clean Bi films prior to

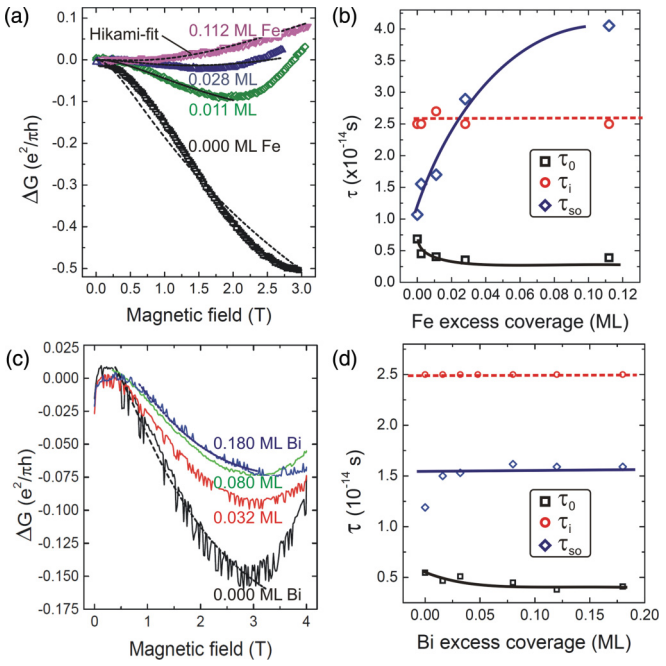

FIG. 5. (Color online) Residual conductance ΔG of data shown in Figs. 3(a) and 2(a) after subtraction of classical contribution for various Fe (a) and Bi (c) coverages. The experimental data can be reliably described by the Hikami theory of weak localization (Ref. 24) (dashed lines). (c) and (d) show the evaluated scattering times deduced from the fits in (a) and (b). There is a change from WAL to WL for Fe on Bi, whereas WAL survives for all Bi excess coverages.

metal adsorption show weak antilocalization, i.e., a decrease of conductance with increasing magnetic field. As is obvious from Figs. 5(a) and 5(c) the WAL signature changes upon adsorption. In the case of Fe adsorption, even the sign of the conductance curve is reversed, i.e., for coverages higher than 0.03 ML the system moves into the weak-localization regime. While this transition is found during adsorption of Co adatoms as well (not shown), for Bi/Bi(111) [Fig. 5(c)] the WAL signature remains present for all excess coverages up to 0.18 ML. Since all adsorbates strongly reduce the mean free paths of the electrons (see above), the WAL-WL transition is clearly related to the magnetic moment of the adsorbates.

In order to quantify the different regimes, characteristic scattering times, i.e., the elastic τ_0, inelastic τ_i, and spin-orbit τ_{so} scattering times, have been deduced from a Hikami analysis[24] (for details the reader is referred to Refs. 15 and 27). The dashed curves in Figs. 5(a) and 5(c) represent best fits. In these fits, τ_i has been kept constant in order to reduce the number of free parameters. The results for Fe and Bi are depicted in Figs. 5(b) and 5(d). As seen there, the elastic scattering time τ_0 decreases gradually as a function of excess coverage, as expected from the data analyzed in the context of Fig. 4. The most remarkable change is seen for τ_{so}, which *increases* by a factor of 4 for Fe (and also Co) adsorption, while it stays constant for Bi. Obviously, Fe leads to a reduction of spin-orbit scattering, in analogy with recent findings in the topological insulator $Bi_{2-x}Cr_xSe_3$ alloyed with magnetic Cr atoms, where a crossover between WAL and WL was found for increasing x.[28] In that work a dramatic change of the band structure and the disappearance of the surface state was observed by angle-resolved photoemission spectroscopy, resulting in WL-like behavior. It is interesting to note that the Fe coverage in our experiment at which signatures of weak localization become obvious in transport is close to the Fe doping concentration in Bi_2Te_3,[30] as discussed in the Introduction.

For Bi/Bi(111) [Fig. 5(d)] only small changes in the scattering times are found. Only τ_0 decreases due to the increasing number of scatterers. Consequently, WAL and the strong spin-orbit coupling characteristic of the Rashba-split surface states are conserved for all excess Bi coverages.

IV. SUMMARY AND CONCLUSION

The change of surface conductivity upon adsorption of Bi, Fe, and Co has been studied by means of macroscopic surface transport measurements. The analysis of Hall and magnetoconductance data has shown that not only does the scattering rate increase (Bi), but also the carrier concentrations are modified in an asymmetric manner, as seen clearly in the cases of Fe and Co adsorption. This can only be explained by modifications of the Fermi surface induced by these adsorbates due to chemical bond formation and by the associated charge transfer. For the clean Bi(111) surface backscattering channels are disabled due to strong spin-orbit coupling and a strongly anisotropic Fermi surface in this system.[14,15,26] As a consequence, the remaining signature of WAL is evident, but small. After adsorption of small amounts of adatoms, acting as impurities, a transition from WAL to WL was found for magnetic atoms [Fe/Bi(111)]. The latter dominates close to 0.1 ML coverage and above. In contrast, the MC curves keep their WAL-like character in the nonmagnetic case [Bi/Bi(111)].

As it turns out, the concept of breaking time-reversal symmetry in the presence of magnetic impurities is too simple. Not only is a critical coverage needed, our data clearly show that the band structure of the Bi(111) surface states must be modified upon adsorption. On the one hand, this requires chemical bond formation, which involves also the *d* electrons of Fe and Co. As a consequence, the original magnetic moment of the Fe and Co atoms is most likely altered upon adsorption on Bi surfaces, and the remaining magnetic moment will depend on details of bond formation, local geometric configuration, etc. These details can be determined only by angle- and spin-resolved photoemission in comparison with quantitative calculations. Such data are still missing for these systems. However, *ab initio* calculations and STM and STS measurements are in agreement with the interpretation given here.[39] On the other hand, the doping levels considered here are already quite high, introducing a considerable amount of disorder into the surfaces, and causing weakening of all surface-symmetry-related selection rules. Which of these effects is dominant and is directly related to the effective magnetic moments of the adsorbates still remainsl to be clarified.

ACKNOWLEDGMENTS

Financial support by the Deutsche Forschungsgemeinschaft (D.L.) and the DAAD (S.S.) is gratefully acknowledged.

*tegenkamp@fkp.uni-hannover.de

[1] E. Y. Tsymbal and D. G. Pettifor, Solid State Physics **56**, 113 (2001).
[2] S. O. Valenzuela and M. Trinkham, Nature (London) **442**, 176 (2006).
[3] S. Datta and B. Das, Appl. Phys. Lett. **56**, 665 (1990).
[4] J. Henk, M. Hoesch, J. Osterwalder, A. Ernst, and P. Bruno, J. Phys.: Condens. Matter **16**, 7581 (2004).
[5] Ph. Hofmann, J. E. Gayone, G. Bihlmayer, Yu. M. Koroteev, and E. V. Chulkov, Phys. Rev. B **71**, 195413 (2005).
[6] H. Dil, J. Phys.: Condens. Matter **21**, 403001 (2009).
[7] K. Yaji, Y. Ohtsubo, S. Hatta, H. Okuyama, K. Miyamoto, T. Okuda, A. Kimura, H. Namatame, M. Taniguchi, and T. Aruga, Nat. Commun. **1**, 1 (2010).
[8] H. C. Manoharan, Nat. Nanotechnol. **5**, 477 (2010).
[9] M. Z. Hasan and C. L. Kane, Rev. Mod. Phys. **82**, 3045 (2010).
[10] Xiao-Liang Qi and Shou-Cheng Zhang, Rev. Mod. Phys. **83**, 1057 (2011).
[11] P. Roushan, J. Seo, C. V. Parker, Y. S. Hor, D. Hsieh, D. Qian, A. Richardella, M. Z. Hasan, R. J. Cava, and A. Yazdani, Nature (London) **466**, 1106 (2009).
[12] J. W. Wells, J. H. Dil, F. Meier, J. Lobo-Checa, V. N. Petrov, J. Osterwalder, M. M. Ugeda, I. Fernandez-Torrente, J. I. Pascual, E. D. L. Rienks, M. F. Jensen, and Ph. Hofmann, Phys. Rev. Lett. **102**, 096802 (2009).
[13] A. Stróżecka, A. Eiguren, and J. I. Pascual, Phys. Rev. Lett. **107**, 186805 (2011).
[14] M. C. Cottin, C. A. Bobisch, J. Schaffert, G. Jnawali, A. Sonntag, G. Bihlmayer, and R. Möller, Appl. Phys. Lett. **98**, 022108 (2011).
[15] D. Lükermann, S. Sologub, H. Pfnür, and C. Tegenkamp, Phys. Rev. B **83**, 245425 (2011).
[16] G. Jnawali, Th. Wagner, H. Hattab, R. Möller, A. Lorke, M. Horn-von Hoegen, e-J. Surf. Sci. Nanotech. **8**, 27 (2010).
[17] G. Jnawali, C. Klein, Th. Wagner, H. Hattab, P. Zahl, D. P. Acharya, P. Sutter, A. Lorke, and M. Horn-von Hoegen, Phys. Rev. Lett. **108**, 266804 (2012).
[18] T. Hirahara, I. Matsuda, S. Yamazaki, N. Miyata, S. Hasegawa, and T. Nagao, Appl. Phys. Lett. **91**, 202106 (2007).
[19] T. Hirahara, T. Nagao, I. Matsuda, G. Bihlmayer, E. V. Chulkov, Yu. M. Koroteev, P. M. Echenique, M. Saito, and S. Hasegawa, Phys. Rev. Lett. **97**, 146803 (2006).
[20] Zheng Liu, Chao-Xing Liu, Yong-Shi Wu, Wen-Hui Duan, Feng Liu, and Jian Wu, Phys. Rev. Lett. **107**, 136805 (2011).
[21] Y. M. Koroteev, G. Bihlmayer, J. E. Gayone, E. V. Chulkov, S. Blügel, P. M. Echenique, and Ph. Hofmann, Phys. Rev. Lett. **93**, 046403 (2004).
[22] S. Xiao, D. Wei, and X. Jin, Phys. Rev. Lett. **109**, 166805 (2012).
[23] N. Miyata, R. Hobara, H. Narita, T. Hirahara, S. Hasegawa, and I. Matsuda, Jpn. J. Appl. Phys. **50**, 036602 (2011).
[24] S. Hikami, A. I. Larkin, and Y. Nagaoka, Prog. Theor. Phys. **63**, 707 (1980).
[25] G. Bergmann, Phys. Rep. **107**, 1 (1984).
[26] N. Miyata, H. Narita, M. Ogawa, A. Harasawa, R. Hobara, T. Hirahara, P. Moras, D. Topwal, C. Carbone, S. Hasegawa, and I. Matsuda, Phys. Rev. B **83**, 195305 (2011).
[27] D. Lükermann, M. Gauch, M. Czubanowski, H. Pfnür, and C. Tegenkamp, Phys. Rev. B **81**, 125429 (2010).
[28] M. Liu, J. Zhang, C.-Z. Chang, Z. Zhang, X. Feng, K. Li, K. He, L. L. Wang, X. Chen, X. Dai, Z. Fang, Q. K. Xue, X. Ma, and Y. Wang, Phys. Rev. Lett. **108**, 036805 (2012).
[29] T. Valla, Z.-H. Pan, D. R. Gardner, Y. S. Lee, and S. Chu, Phys. Rev. Lett. **108**, 117601 (2012).
[30] Y. Okada, C. Dhital, W. Zhou, E. D. Huemiller, H. Lin, S. Basak, A. Bansil, Y.-B. Huang, H. Ding, Z. Wang, S. D. Wilson, and V. Madhavan, Phys. Rev. Lett. **106**, 206805 (2011).
[31] C. Tegenkamp, D. Lükermann, S. Akbari, M. Czubanowski, A. Schuster, and H. Pfnür, Phys. Rev. B **82**, 205413 (2010).
[32] M. Kammler and M. Horn-von Hoegen, Surf. Sci. **576**, 56 (2005).
[33] R. Shioda, A. Kawazu, A. A. Baski, C. F. Quate, and J. Nogami, Phys. Rev. B **48**, 4895 (1993).
[34] T. Nagao, J. T. Sadowski, M. Saito, S. Yaginuma, Y. Fujikawa, T. Kogure, T. Ohno, Y. Hasegawa, S. Hasegawa, and T. Sakurai, Phys. Rev. Lett. **93**, 105501 (2004).
[35] F. Pang, X.-J. Liang, Z.-L. Liao, S.-L. Yin, and D.-M. Chen, Chin. Phys. B **19**, 087201 (2010).
[36] F. Komori, S. Kobayashi, and W. Sasaki, J. Phys. Soc. Jpn. **52**, 368 (1982).
[37] Y. F. Komnik, I. B. Bertkutov, and V. V. Andrievskiĭ, Low Temp. Phys. **31**, 326 (2005).
[38] A. B. Pippard, *Magnetoresistance in Metals* (Cambridge University Press, Cambridge, 1989).
[39] U. Gerstmann, W. G. Schmidt, C. Klein, M. Horn-von Hoegen *et al.* (unpublished).